Crystallographic Characteristics of Plasma-Sprayed Calcium Phosphate Coatings on Ti-6Al-4V

Eser Tufekci, DDS, MS, PhD*/William A. Brantley, PhD**/John C. Mitchell, PhD***/
Dennis W. Foreman, PhD****/Frederick S. Georgette, MS*****

The purpose of this study was to investigate the crystallographic characteristics of 3 sets of plasma-sprayed hydroxyapatite (HA) coatings prepared with different degrees of crystallinity on Ti-6Al-4V substrates. X-ray diffraction analyses were performed on the coatings to determine mean percent crystallinity, calcium phosphate phases present, average crystallite size, and residual strain. The mean percent crystallinity for the 3 sets of coatings ranged from 49 to 60%. The coatings that achieved the highest crystallinity consisted almost entirely of HA. As the coating crystallinity decreased, increasing amounts of α- and ß-tricalcium phosphate and tetracalcium phosphate were detected. The mean HA crystallite size for the 3 sets of coatings ranged from 0.02 to 0.05 µm. Differences in mean interplanar spacing for selected crystallographic planes of HA, compared with the pure ICDD (International Center for Diffraction Data) powder standards, implied that the coatings were in an uneven state of tensile strain.
(Int J Oral Maxillofac Implants 1999;14:661–672)

Key words: crystallinity, hydroxyapatite, plasma-spraying, titanium, x-ray diffraction

Over the past decade, bioactive calcium phosphate ceramics have been used widely in clinical implant applications because of their biocompatibility and their intimate contact with bone.[1–3] Hydroxyapatite (HA) and tricalcium phosphate (TCP) have been recognized as bioceramics that provide scaffolds upon which bone can grow,[4–7] although they have created some controversy in the dental and orthopedic fields.[8] One drawback of these bioceramics is their brittleness, which results in low impact resistance and tensile strength.[3,4,9] As a solution to this problem, thin coatings of bioceramics on metallic substrates have been introduced, thus combining the strength of metals with the favorable properties of bioceramics.[2,9–11]

The chemistry of calcium phosphate ceramics under equilibrium conditions has been studied extensively.[9,12,13] Synthetic HA is widely used as an implant material because of its structural similarities with biologic HA, the principal natural component of human vertebrate hard tissue (eg, enamel and bone). Biologic hydroxyapatites are deficient in calcium, nonstoichiometric, and may contain minor and trace inorganic elements.[14] Natural HA may have a monoclinic structure because of the strains and distortions resulting from these factors, whereas synthetic pure HA has a hexagonal structure with a chemical formula of $Ca_{10}(PO_4)_6(OH)_2$ and a Ca:P ratio of 1.67. The other calcium phosphate bioceramic commonly used for clinical applications is ß-TCP, also termed *whitlockite*. This bio-

*Former Doctoral Graduate Student, Oral Biology, The Ohio State University, Columbus, Ohio.
**Professor, Section of Restorative Dentistry, Prosthodontics and Endodontics, and Director, Graduate Program in Dental Materials, The Ohio State University, Columbus, Ohio.
***Former Doctoral Graduate Student, Biomaterials Implant Science/Tissue Engineering and Adjunct Instructor/Senior Electron Microscopist, Microscopic and Chemical Analysis Research Center, Department of Geological Sciences, The Ohio State University, Columbus, Ohio.
****Professor Emeritus, Oral Biology and Geological Sciences, The Ohio State University, Columbus, Ohio.
*****President, Bio-Coat, Southfield, Michigan.

Reprint requests: Dr William A. Brantley, Section of Restorative Dentistry, Prosthodontics and Endodontics, College of Dentistry, The Ohio State University, 305 West 12th Avenue, Columbus, OH 43210-1241. Fax: 614-292-9422.

From a portion of a dissertation submitted to the Graduate School of The Ohio State University for the degree of Doctor of Philosophy.

ceramic also has a hexagonal structure with a chemical formula of $Ca_3(PO_4)_2$ and a Ca:P ratio of 1.50. Variations in Ca:P ratios and substitution of other ions such as fluorine result in differences in solubility and bone bonding.[11,15]

Plasma spraying is the technique currently favored by manufacturers for forming dense, adherent coatings of HA/TCP ceramics on metal substrates.[11,16,17] Plasma spraying of molten particles results in a highly textured coating because of incomplete coalescence of splat deposition sites; this is considered to be beneficial in providing mechanical interlocking and improved bonding of bone to the implant surface.[18–20] However, during the coating process, as a result of the highly nonequilibratory nature of the plasma spraying technique and the very high plasma temperatures (in excess of 10,000°C), the starting powder particles, such as HA and TCP, experience structural changes.[4,10,21,22]

X-ray diffraction (XRD) studies have confirmed that plasma spraying induces phase compositional and crystal structural changes in the starting powder particles, thereby influencing the in vivo stability of the coatings.[3,10,21,23–25] Since there is almost always phase transformation during the plasma spraying process, it would be more appropriate to use the general term *calcium phosphate ceramics* for the bioceramic coatings. It is found that under equilibrium conditions, HA transforms mainly into ß-TCP around 1300°C, and the transition temperature between the α and ß phases of TCP occurs around 1200°C.[10,21,25] The nonequilibrium plasma-sprayed coatings can contain various crystalline phases (HA, ß-TCP, α-TCP, calcium pyrophosphate [PP], tetracalcium phosphate [TTCP], and calcium oxide [CaO]), as well as an amorphous (glassy) calcium phosphate phase (ACP).[4,10,21,26,27]

Despite their beneficial roles in providing improved bone/implant contact and preventing possible leakage of metal ions from the substrate,[28,29] the in vivo stability of these coatings has been questioned because of the nonequilibrium conditions during plasma spraying. Based on the foregoing results, one may expect dissolution or instability of the coatings in vivo,[21,25,30] and it is essential to clarify that their biocompatibility and dissolution are within an acceptable range. Numerous studies have shown that the tendency for biodegradation of the calcium phosphates occurs in the following order[12,13]: ACP > TTCP >> α-TCP > ß-TCP >> HA. Therefore, the crystallinity and composition of the coatings, as well as microscopic and residual stresses, are believed to affect the biologic and mechanical behavior of the implants.[3,10,20,24,30] Residual stresses, which may occur as the result of rapid cooling rates and differences in the coefficients of thermal contraction of the coating and the substrate, can cause surface cracking and delamination in the coatings. Eventually, these stresses can lead to the detachment of the coating in service.

The purpose of this study was to use an x-ray diffractometric technique to characterize the crystallographic nature of calcium phosphate coatings plasma-sprayed onto Ti-6Al-4V coupons under different conditions. Hydroxyapatite crystal size in the coatings was determined from the full width at half-maximum (FWHM) intensity of selected reflection planes, and comparison of the HA peak positions to those of an appropriate standard provided information about residual strain in the coatings.

Materials and Methods

For this study, 1 inch × 1 inch × 0.25 inch flat coupons of Ti-6Al-4V alloy were custom plasma-sprayed, using pure HA starting powder (> 99 wt %) and proprietary processes (Bio-Coat, Southfield, MI). Three groups of samples (n = 3) were prepared with different degrees of coating crystallinity, and labeled as A, B, and C. The plasma spraying parameters for the Group A coatings were representative of those used for dental and orthopedic implants commercially available in the market. However, for the Groups B and C coatings, the distance from the plasma-spraying gun to the specimen was deliberately changed for scientific study. For these 2 groups, the stand-off distance was increased, with a larger distance for the Group C specimens. Gross et al[7] have suggested that a larger distance between the plasma gun and the object to be coated will result in thicker splats, yielding a higher amount of amorphous phase formation.

In the first part of this study, nondestructive XRD analyses were performed on the intact coatings over a diffraction angle (2θ) range of 15 to 45 degrees, using Cu Kα radiation (weighted average λ = 1.542 Å for Cu $K\alpha_1$ and Cu $K\alpha_2$)[31] and a Philips Electronics PW 1316/90 wide-range goniometer (Eindhoven, The Netherlands) with XRG 3100 x-ray generator, DMS-41 measuring system, θ-compensating slit, and graphite monochromator. This high-precision apparatus was periodically calibrated using known crystallographic standards. The 2θ step interval was 0.05 degrees with a counting time of 10 sec/step. Additional XRD analyses over the range 15 to 85 degrees were also run on 1 sample each from Groups A

and C. An XRD analysis between 34 and 78 degrees was performed on the back side of 1 specimen from the C group to obtain the most intense peaks from the titanium alloy substrate to aid in the peak assignments.

The coated flat coupons were further analyzed in novel XRD experiments in the second part of the study to determine the residual stresses in the coatings. For these experiments, a small amount of tungsten powder was carefully sprinkled over each specimen surface to serve as a control to standardize the positions of the XRD peaks. Previous calibration experiments had shown that the positions of the XRD peaks from this powder closely matched those from the ICDD (International Center for Diffraction Data, Swarthmore, PA) for tungsten. The position of the strongest (110) peak from tungsten (as an internal experimental standard) was used to determine the instrumental shift of the peak positions for the calcium phosphate phrases in each coating from the positions given in the ICDD standards. These XRD analyses were performed over a 2θ range of 10 to 80 degrees using CuKα radiation, a 2θ-step interval of 0.02 degree, and a counting time of 3 sec/step.

The full XRD patterns for the coatings in the first part of the study, where the tungsten powder was not used, were examined using a computer program written by one of the authors[32] to determine the mean 2θ peak positions, the FWHM intensity for these peaks, and the average crystallite size, as well as the phases present and the degree of crystallinity. This computer program fit diffractometric data pairs (2θ, counts) to a Gaussian distribution, using a weighted regression analysis, which also provided an assessment for experimental errors. Because of their highly symmetric Gaussian shape, the (002), (210), and (202) reflections for HA were further analyzed to determine the state of residual stresses and crystallographic differences in the coatings of different groups. The average HA crystallite sizes were obtained from the Debye-Scherrer formula[31]:

$$r = \frac{K\lambda}{B\cos\theta} \qquad \text{(Equation 1)}$$

where r is the crystallite dimension (Å) in the direction perpendicular to the chosen crystallographic plane, K is a constant (0.9), λ is the wavelength of the Cu Kα x-rays, and B is the observed broadening measured in radians at the half-maximum height of the XRD peak. If the instrumental broadening (B_i) is known, it can be included in Equation 1 to account for the true broadening.[31] The line broadening may indicate crystallite size and crystallite strain if there is nonuniform deformation.

The percent crystallinity (%C) (ie, the total percentage of all of the crystalline phases in the coating) was calculated using the following equation[32]:

$$\%C = \frac{100I_{xtl}}{I_{xtl} + I_{am}} \qquad \text{(Equation 2)}$$

where I_{am} is the total intensity arising from the amorphous phase and I_{xtl} is the total intensity arising from the several crystalline phases in the coating. The value of I_{xtl} was obtained by integrating the area under the crystalline reflections between 15 and 45 degrees (2θ) of the background-corrected-intensity XRD pattern. The amorphous phase was identified by a broad hump near 30 degrees. The value of I_{am} was obtained by fitting the curve for the intensity of this ACP component into a linear expression (over the 2θ range of 15 to 29 degrees) and a fourth-order polynomial expression (over the 2θ range of 29 to 45 degrees) and integrating over the range of the amorphous contribution.[32] (Other mathematical relationships were also tried, but the linear and polynomial combination of expressions yielded the highest correlation coefficient.) The mean percent crystallinity was calculated using those selected reflecting planes for each of the 3 specimens from the 3 groups (n = 3). The principles behind this computer program have been used by other investigators for the study of HA coatings.[7,33,34] The numerical procedures were facilitated by the use of computer software (PSI-Plot, Poly Software International, Salt Lake City, UT). For identification of the phases in the coatings, the XRD patterns were compared with files of appropriate ICDD polycrystalline powder standards. If the difference between the interplanar spacings (d-spacings) calculated from observed 2θ values and the d-spacings for the standard were ≤ 0.03 Å, then the match was considered to be good.

The mean values of 2θ, FWHM, r, and %C for Groups A, B, and C were compared statistically using 1-way analysis of variance (ANOVA) (n = 3). A level of $\alpha = .05$ was chosen as the criterion for statistical significance.

As previously noted, in the second part of the study, tungsten powder served as an internal standard for the determination of the instrumental shift of the x-ray diffractometer system, which was also taken into consideration in the calculations of the residual stresses in the coatings. The peak positions and FWHM values for the (002), (210), and (202) planes were determined using the commer-

cially available Peak-Fit computer program (SPSS, Chicago, IL). The changes in interplanar spacing for these selected planes compared to the ICDD powder standard for HA were again used to calculate the strains, and crystallite sizes were calculated using Equation 1. The data obtained with the Peak-Fit software were compared to those obtained from the first part of the study, where a different computer program written by one of the authors[32] was used.

Results and Discussion

The XRD patterns obtained from representative coatings from the 3 groups are shown in Figs 1 to 3. Comparing the relative sizes of the broad background crests from the ACP phases, it is evident that Group A had the highest crystallinity, Group B was intermediate, and Group C had the lowest crystallinity. The XRD patterns obtained from Group A specimens exhibited the strongest and sharpest peaks, whereas Group C specimens had the weakest and broadest peaks. There were some small peaks that were not readily visible for Group A but became increasingly prominent for Groups B and C as the crystallinity decreased. These qualitative observations were confirmed by quantitative analyses of the XRD patterns, where calculated d-spacing values were compared with ICDD standards to identify reflecting planes.

Results indicated that coatings in Group A consisted mainly of HA and the amorphous (ACP) phase. All of the major peaks in Fig 1 were found to correspond to ICDD standard 9-432 (Table 1) for HA, and there was very good agreement within about 0.01 Å for the calculated d-spacings and the ICDD standard. The good qualitative agreement between the relative intensities for the peaks and those in the standard indicated that there was little preferred orientation for the HA in the coatings. There were also some weak additional peaks, but difficulties in distinguishing these peaks from the background and the small number of data pairs in each peak precluded accurate determinations of mean 2θ values. Nevertheless, the positions of these weak peaks (Fig 1) closely matched those of ICDD standard 29-359 (Table 1) for α-TCP.

Groups B and C contained XRD peaks that could generally be indexed to multiple calcium phosphate phases (Figs 2 and 3). Referring to the example in Table 2, the coatings in these 2 groups contained TTCP (ICDD 25-1137), α-TCP (ICDD 29-359), and ß-TCP (ICDD 9-169), in addition to HA. Lattice parameters corresponding to the calcium phosphate phases in the coatings are summarized in Table 1. Because of their very similar compositions and peak positions in the ICDD standards, the presence of other calcium phosphate phases, such as calcium pyrophosphate ($Ca_2P_2O_7$) and octacalcium phosphate [$Ca_8H_2(PO_4)_6 \cdot 5H_2O$], cannot be precluded. An XRD scan extending from 15 to 85 degrees was also performed for 2 representative coatings to provide maximum accuracy for the peak assignments to specific phases. Since there also appeared to be little preferred orientation for the HA in Groups B and C, if some of the strong reflecting planes for a particular phase were missing, it was assumed that this phase was not present in the coating. For example, if the peak at 2θ = 29.40 degrees and a relative intensity of 100 were assigned to α-PP (ICDD 9-345), then another strong peak at 27.68 degrees should also be present. However, Table 2 shows that this peak was missing.

For the same reason, it could not be concluded that the CaO phase was present in the coatings, although some possible reflections were observed (Table 2). Upon examination of the entire XRD pattern, this phase was ruled out because of many missing reflections. Nevertheless, other studies[11,30] have shown that CaO is present in plasma-sprayed HA coatings. This is plausible since high temperatures can cause dehydroxylation of HA, which could lead to formation of this phase.

One major problem encountered in matching the diffraction patterns to ICDD standards, so as to determine whether phases other than HA were present, was the frequent overlapping of the XRD peaks. For example, the majority of strong peaks from TTCP were masked by the more intense HA peaks. However, the strongest peak for TTCP (as well as other weak peaks) was present throughout the XRD patterns for coatings from Groups B and C, which suggested that this phase was present. Since comparison of the relative intensities for the HA peaks in the coatings with the ICDD standard suggested minimal preferred orientation, another criterion for phase identification was agreement of the relative peak intensities for each possible phase in a coating with those for the peaks in the ICDD standard. While preferred orientation might be expected at the coating/titanium alloy interface because of epitaxial effects, this is unlikely in the bulk coating because of the random nature of the plasma deposition process and insufficient time available for growth kinetics. It was concluded that, as the coating crystallinity decreased from Group A to Group C, α-TCP, ß-TCP, and TTCP were present in increasing amounts. These results are not surprising, since very high temperatures

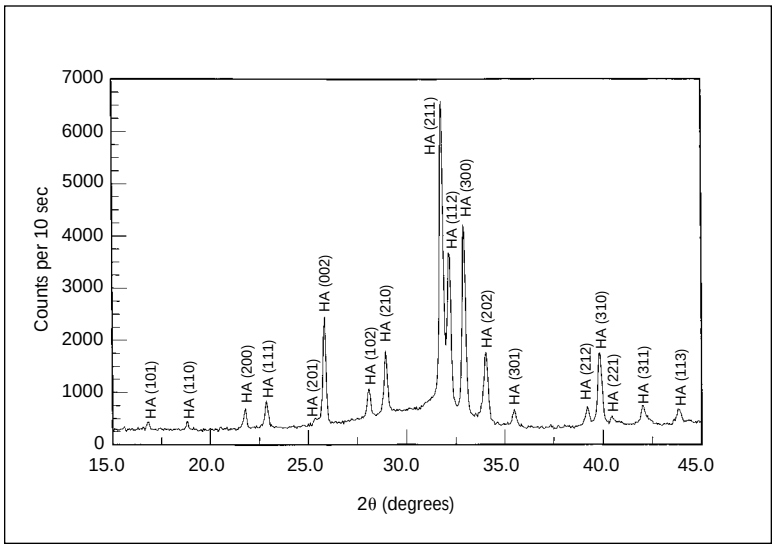

Fig 1 X-ray diffraction pattern of specimen 1 from Group A, showing the peaks that correspond only to HA.

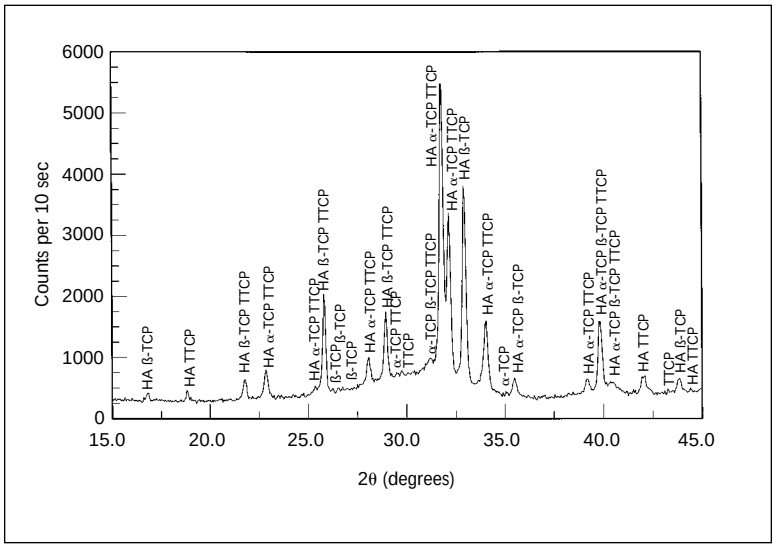

Fig 2 X-ray diffraction pattern of specimen 1 from Group B, showing the peaks that correspond to other phases in addition to HA.

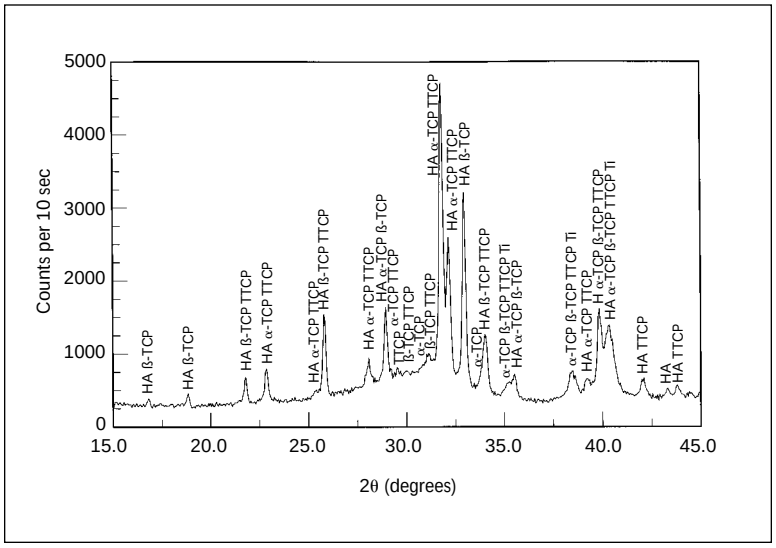

Fig 3 X-ray diffraction pattern of specimen 1 from Group C, showing the peaks that correspond to other phases in addition to HA.

Table 1 Lattice Parameters for the Calcium Phosphate Phases in the Coatings

Phase	Structure	Lattice Parameters	Ca:P molar ratio	Reference (ICDD)
HA	Hexagonal	a = 9.418 Å c = 6.884 Å	1.67	9-432
α-TCP	Monoclinic	a = 12.887 Å b = 27.280 Å c = 15.219 Å ß = 126.2 deg	1.50	29-359
ß-TCP	Rhombohedral*	a = 10.429 Å c = 37.380 Å	1.50	9-169
TTCP	Monoclinic	a = 7.018 Å b = 11.980 Å c = 9.469 Å ß = 90.88 deg	2.00	25-1137

*The axial angle for this crystal structure was not provided in the ICDD standard.

Table 2 Possible Assignments of the XRD Peaks for Specimen 1 from Group C

Intensity (counts/10 sec)	2θ (degrees)	d (Å)	Interpretation
390	16.800	5.277	Good match: HA; poor match: ß-TCP, OCP
461	18.811	4.718	Good match: HA, TTCP, ß-PP, OCP
684	21.753	4.086	Good match: HA, ß-TCP, TTCP, OCP
798	22.853	3.892	Good match: HA, α-TCP, TTCP; poor match: ß-TCP, OCP
510	25.400	3.507	Good match: HA, α-TCP, TTCP; poor match: ß-TCP, ß-PP
1544	25.814	3.452	Good match: HA, ß-TCP, TTCP, α-PP, OCP
944	28.087	3.177	Good match: HA, α-TCP, ß-TCP, TTCP, α-PP, OCP
1637	28.969	3.082	Good match: HA, α-TCP, ß-TCP, TTCP, α-PP, ß-PP, OCP
800	29.199	3.058	Good match: α-TCP, TTCP, ß-PP, OCP; poor match: ß-TCP
753	29.397	3.038	Good match: α-TCP, ß-TCP, TTCP, ß-PP, OCP, CaO
826	29.550	3.023	Good match: α-TCP, ß-TCP, TTCP, ß-PP, OCP, CaO
1006	31.150	2.871	Good match: α-TCP, ß-TCP, OCP
4710	31.749	2.818	Good match: HA, α-TCP, TTCP, ß-PP, OCP
2600	32.150	2.784	Good match: HA, α-TCP, ß-TCP, TTCP, α-PP, ß-PP, OCP
3211	32.941	2.719	Good match: HA, ß-TCP, TTCP, OCP
1269	33.989	2.638	Good match: HA, ß-TCP, TTCP, α-PP, OCP
612	35.250	2.546	Good match: α-TCP, ß-TCP, TTCP, α-PP, ß-PP, OCP
721	35.500	2.529	Good match: HA, ß-TCP, α-PP, ß-PP; poor match: α-TCP
761	38.504	2.338	Good match: α-TCP, TTCP, OCP; poor match: ß-TCP
702	38.600	2.332	Good match: α-TCP, TTCP, OCP; poor match: ß-TCP
656	39.255	2.295	Good match: HA, TTCP; poor match: α-TCP, OCP
1615	39.850	2.262	Good match: HA, α-TCP, ß-TCP, TTCP, ß-PP, OCP, CaO; poor match;α-PP
1391	40.338	2.236	Good match: HA, ß-TCP, TTCP, ß-PP; poor match: α-TCP
672	42.059	2.148	Good match: HA, TTCP, α-PP, ß-PP
527	43.312	2.089	Good match: ß-TCP, TTCP, α-PP, ß-PP, OCP, CaO
564	43.815	2.066	Good match: HA, ß-TCP, TTCP, α-PP, ß-PP, OCP

HA = hydroxyapatite; α- and ß-TCP = α- and ß-tricalcium phosphate; TTCP = tetracalcium phosphate; α- and ß-PP = α- and ß- pyrophosphate; OCP = octacalcium phosphate; CaO = calcium oxide.

(> 10,000°C) are generated in the plasma gun and the molten powder particles are directed onto the substrate by the ionized carrier gas (plasma) in milliseconds.[35] Because of the highly nonequilibrium conditions during plasma spraying, dehydroxylation and phase transformations of the starting powder particles can occur.[11]

A noteworthy result was the presence of α-titanium peaks (ICDD 5-682) in the coatings of Group C. The identity of these peaks was confirmed on the extended XRD patterns and by obtaining an XRD pattern from the uncoated back of one Ti-6Al-4V coupon. To verify whether the x-rays traveled a sufficient distance through the bulk coating to the titanium alloy substrate, depth-of-penetration calculations were carried out using the following formula[36]:

$$x = \frac{K_x \sin\theta}{2\mu} \qquad \text{(Equation 3)}$$

where μ is the linear absorption coefficient (for HA), θ is the x-ray angle of incidence (half the diffraction angle in Figs 1 to 3), and K_x is a tabulated constant based on the fraction (G_x) of the total diffracted intensity contributed by a surface layer of depth (x).

These calculations showed that the x-ray path lengths through the coatings required to yield peaks from the substrates were plausible. For example, at a 2θ value of 40 degrees and assuming that 99% of the x-rays were collected, the distance that the x-ray beam would need to travel to reach the substrate was about 50 μm. Even though the actual coating thickness of the specimens was not known, it was assumed to be around 50 μm, the optimum thickness desired by manufacturers.[2,10,21] Therefore, the XRD pattern is believed to arise from the bulk coating. The present results indicate that the 3 specimens in Group C had a lower coating thickness than the specimens belonging to Groups A and B, which did not exhibit titanium peaks in their XRD patterns.

When the XRD pattern obtained from the back of a coupon in Group C was carefully examined, peaks in addition to those for α-titanium were present. These extra peaks were indexed to alumina (ICDD 42-1468). Previous investigations of the microscopic and morphologic features of calcium phosphate–coated dental implants showed aluminum-rich particles at the coating/substrate interface, as revealed by x-ray energy-dispersive analysis with the scanning electron microscope,[37,38] and these particles were identified as alumina using x-ray wavelength-dispersive analysis with the electron microprobe.[39] Apparently, alumina particles become entrapped in the titanium alloy substrate during grit blasting, a process employed by manufacturers to achieve a rough surface on the substrate and improve coating adherence.

Table 3 Percent Crystallinity Results for the 3 Groups of Coatings*

Specimen	Group A	Group B	Group C
1	61	50	54
2	56	57	43
3	64	46	49
Mean (SD)	60 (4)	51 (6)	49 (6)

*n = 3; values were not significantly different ($P > .05$).

The percent crystallinity calculations obtained with the computer program used by Foreman and Jakes,[32] which are provided in Table 3, confirmed that Group A had the highest crystallinity, with a value of 60 ± 4% (mean ± standard deviation). Independent measurements (Lambda Research, Cincinnati, OH) on coatings nominally identical to those in Group A yielded a mean percent crystallinity of 65.1%. Group B had crystallinity of 51 ± 6%, and Group C had crystallinity of 49 ± 6%. Previously, Lacefield[4] and LeGeros et al[13] reported crystallinity ranges in plasma-sprayed coatings of 40 to 80% and 30 to 70%, respectively. However, it is well known that these results are highly dependent upon the method used to analyze the XRD patterns, and independent laboratories report different values of percent crystallinity for the same specimens. The percent crystallinity results are based upon all of the phases present in the coatings, and they represent the ratio of the total amount of crystalline phases to the sum of the crystalline and amorphous phases, as shown in Equation 2. The contribution of the secondary crystalline calcium phosphate phases to the percent crystallinity was minor, since these phases had weak peaks compared to the large HA peaks. There were no significant differences among the 3 coating groups ($P > .05$) for the percent crystallinity results. A larger sample size may be needed to show statistical differences between the groups, since the sample size in this study was relatively small (n = 3 for each group).

In the second part of this study, the state of stress in the coatings was investigated with particular care, since the presence of residual stresses may contribute significantly to the bond strength with the substrate as measured with conventional

Table 4 Mean Values and Standard Deviations of 2θ, FWHM, and *r* for Groups A, B, and C from the (002), (210), and (202) Reflecting Planes Obtained Using 2 Techniques

	Group A			Group B			Group C		
	(002)	(210)	(202)	(002)	(210)	(202)	(002)	(210)	(202)
Mean 2θ	25.82	28.95	34.01	25.81	28.96	34.00	25.82	28.98	34.00
(deg)*	(0.01)	(0.00)	(0.01)	(0.00)	(0.02)	(0.01)	(0.00)	(0.01)	(0.02)
FWHM	0.21	0.25	0.32	0.21	0.34	0.34	0.21	0.36	0.31
(deg)*	(0.03)	(0.07)	(0.03)	(0.07)	(0.00)	(0.00)	(0.00)	(0.00)	(0.03)
r (Å)*	396	351	258	412	239	290	396	228	274
	(69)	(110)	(28)	(110)	(0)	(0)	(69)	(20)	(28)
Mean 2θ	25.86	28.98	34.08	25.85	28.98	34.06	25.84	28.99	34.04
(deg)†	(0.00)	(0.01)	(0.08)	(0.02)	(0.01)	(0.02)	(0.00)	(0.01)	(0.01)
FWHM	0.18	0.26	0.24	0.25	0.26	0.26	0.20	0.28	0.27
(deg)†	(0.01)	(0.00)	(0.02)	(0.12)	(0.08)	(0.06)	(0.02)	(0.06)	(0.02)
r (Å)†	481	325	351	397	344	332	417	305	308
	(10)	(43)	(31)	(165)	(96)	(72)	(36)	(67)	(21)

*Data obtained using the computer program developed by Foreman.[32]
†Data obtained using the Peak-Fit software.

mechanical tests.[2,22] The relatively sharp (002), (210), and (202) planes for HA were analyzed (Fig 1). As can be seen in Table 4, there was high precision in the 2θ and FWHM values obtained for the 3 different coating groups in the first part of the study. While it was felt that the use of tungsten as an internal standard in the second part of the study gave more precise data, Table 4 shows that similar values were obtained in both parts of the study for the standard deviations of the 2θ and FWHM values. The crystallite size (*r*) for each of the 3 coating groups, defined as the average size of a region that has the same coherently diffracting structure,[21] exhibited a wide range of values for the (002), (210), and (202) reflecting planes. For example, the mean value of *r* for Group B was 412 Å and 239 Å for the (002) and (210) reflecting planes, respectively. Nevertheless, the present range for *r* in Table 4 was less than that in a previous study,[21] which also reported the differences in crystallite size for various reflecting planes. It was suggested[21] that the different values of *r* arise from the structural properties of the crystalline starting HA powder and the conditions of deposition onto the substrate. Because of several relatively large standard deviations, there were no significant differences in *r* among the 3 coating groups ($P > .05$), and the mean crystallite size ranged from 0.02 to 0.05 μm.

Table 4 indicates minimal variation (usually not exceeding 0.01 degree) between the values of mean 2θ for each of the 3 reflecting planes among the 3 coating groups. This result not only verified the high precision of the diffractometric technique, but also suggested that there was little difference in the purity or stoichiometry of the HA phase in the 3 coating groups. While the positions and relative intensities of the XRD peaks for the HA phase in the coatings were in excellent agreement with ICDD standard 9-432, comparisons of mean 2θ values for HA in Table 4 to those computed from the interplanar spacings for the pure ICDD powder standard imply an uneven state of strain in the coatings. Both XRD techniques in the present study (ie, using or not using tungsten powder as an internal standard) showed that the coatings were under both tensile and compressive stresses, although generally the stresses were tensile. This is not surprising, since the higher reported thermal contraction coefficient for HA compared to the Ti-6Al-4V substrate creates residual tensile stresses in the coating parallel to the interface, and cracks will appear if the residual stress exceeds the tensile strength of the coating.[40,41] Previous studies have shown that plasma-sprayed coatings have numerous surface cracks.[37–39] Even though the (002), (210), and (202) XRD peaks from the HA were sharp, overlapping reflections from other crystalline phases in Groups B and C might contribute uncertainty to the results for these specimens. More detailed study using sophisticated XRD stress measurement techniques[36] is required to investigate the stresses in the coatings.

In this study, the residual strains for the selected reflecting planes were estimated using the following formula:

$$\epsilon = \frac{d_o - d_s}{d_s} \qquad \text{(Equation 4)}$$

where ϵ is the strain for the reflecting plane considered, d_o is the observed interatomic spacing, and d_s is the interatomic spacing according to the ICDD standard for that reflecting plane. The very small strain values ranged over an order of magnitude between 0.0003 and 0.0035 and were nearly at the limit of detection for the XRD technique used in this study. Residual stresses were calculated using the relationship for the applicable case of 2-dimensional plane stress[42]:

$$\sigma = \frac{E\epsilon}{1 - \nu} \qquad \text{(Equation 5)}$$

where σ is the stress; E and ν are the modulus of elasticity (34 GPa)[40] and Poisson's ratio (0.28)[43] of HA, respectively, and ϵ is the strain for parallel members of the given reflecting plane. This relationship is derived from the assumption that the normal stresses (σ_x and σ_y) in the plane of the coating are approximately equal because of the square specimen geometry and isotropic properties of the coating. The third normal stress (σ_z) is assumed to be zero because of the very small coating thickness. Therefore, the coatings are considered to be in a 2-dimensional state of plane stress.[44]

Values of residual stresses obtained from the first and second parts of this study for the (002), (210), and (202) reflecting planes ranged from 10 to 120 MPa and 0 to 136 MPa, respectively. Since the use of high-angle XRD peaks is desirable to achieve stress measurements with an increased sensitivity to small changes in the d-spacing and to reduce instrumental errors,[45] the stresses for the (004) and (513) reflecting planes were also examined. The mean stress values for the (004) reflecting plane were 0 MPa, 63 ± 27 MPa, and 0 MPa for Groups A, B, and C, respectively. For the (513) reflecting plane, the mean stress values were found to be 100 ± 21 MPa, 63 ± 98 MPa, and 31 ± 98 MPa, respectively, for the same 3 coating groups. The stresses were found to be in both the tensile and compressive states. Since there was a substantial scatter in the data, larger sample sizes might be needed to more accurately determine the stresses, although it is still likely that such results would have high variability. It should be noted that back-reflection peaks ($2\theta > 90$ degrees) for the most accurate stress determination are not available for HA when Cu Kα x-rays are used.

Nonetheless, the values of residual stress found in the present study were comparable to the reported tensile strength values (40 to 80 MPa) of HA.[46,47] The wide range of values published for both the elastic modulus and tensile strength of HA[40,46–48] is not unexpected, since these mechanical properties are highly dependent upon the method of processing.[49] Sergo et al[50] pointed out that, although calculated residual stress values are around 440 MPa, the difference in the coefficients of contraction between the coating and the substrate causes the actual stresses to be less than the theoretical values. They concluded that residual stresses are also dominated by growth conditions that result in smaller values (approximately 100 MPa).

LeGeros[14] emphasized that there is an additional contribution to the XRD peak broadening, which is proportional to both the strain and tan θ. For the data in Table 2 and a hypothetical situation of uniform strain, there would be a broadening of approximately 34% for the (202) peak compared to the (002) peak. In the present experiments, the observed peak broadening, which was used to calculate crystallite size (r) with Equation 1, had the opposite trend of being greater for the (002) peak than for the (202) peak. Because of the uneven stress conditions prevailing in the HA coatings, correction of the mean values of (r) in Table 4 was not possible.

The residual stress developed in the coating during cooling may first be crudely estimated using the following formula,[51] assuming that the substrate acts as a rigid (noncontracting) material during this process:

$$\sigma = E\alpha(T_g - T) \qquad \text{(Equation 6)}$$

where E and α are the modulus of elasticity (34 GPa)[40] and thermal contraction coefficient (11×10^{-6}/°C),[40] respectively, of HA, T_g is the glass transition temperature, and T is the temperature of interest. The glass transition temperature is a very important factor in determining the stresses that occur during cooling of the ceramic. Above T_g, viscous flow in the ceramic is capable of relieving any stress, whereas below T_g the material behaves as an elastic solid, and stress relaxation does not take place.[52] In the absence of published data on the glass transition temperature of HA, T_g was assumed to be around 600°C, which is the glass transition temperature of dental porcelain.[52] Using this value in the above relationship, the residual stress in the coatings is estimated to be 215 MPa, which is much higher than the range of values found from the XRD analysis.

Alternatively, residual stress calculations may be performed based on the assumption that the titanium alloy substrate also contracts during the cooling process for the coating. This is a more complex situation, since the thermal and mechani-

cal properties of both materials need to be taken into consideration. In this case, tensile stresses will be created in the coating, while compressive stresses will be created in the substrate, as a result of the lower value of α (8.6×10^{-6}/°C)[40] for titanium. There will be a mechanical equilibrium where equal and opposite stresses occur in the coating and substrate. This equilibrium point may be derived using the following basic formula[51]:

$$l_f = l_o[1 - \alpha(\Delta T)] \qquad \text{(Equation 7)}$$

where l_f and l_o are the final and original lengths, α is the thermal contraction coefficient, and ΔT is the difference in the final and starting temperatures (room temperature and T_g). Once the length of the materials at equilibrium (l_e) is obtained, the residual stress may be calculated from the value of strain resulting from the difference between l_e and the length that would occur if the coating were not bonded to the substrate. However, because of the relatively thin coating (50 µm) and thick substrate (3 mm), the coating will be in a state of plane stress (where the elastic modulus can be calculated as $E/[1 - \nu]$) and the substrate will be in a state of plane strain (where the elastic modulus can be calculated as $E/[1 + \nu]$).[40,43] In this case, the residual stress in the coating was found to be 121 MPa, which is within the range obtained from the XRD analyses. These latter calculations may represent the true situation, since the Ti-6Al-4V substrate surface is in contact with the molten ceramic particles at high temperatures (T_m = 1600°C)[49] and should be subject to some thermal contraction.

Other analytic techniques, such as Fourier transform infrared analysis and Raman spectroscopy, can provide additional information such as the loss of OH from HA, which is not readily determined using XRD.[4] It has been reported that the same information can be obtained from powder XRD patterns studied by the Rietveld method. In this technique, a powder pattern is analyzed on the basis of both a structural model and the characteristics of the instrument used, and the differences between the observed and calculated intensities are minimized.[53]

This study has shown that proprietary plasma spraying of current dental implants results in calcium phosphate coatings containing approximately 50 to 60% crystalline HA, with small amounts of other crystalline phases (α-TCP, ß-TCP, and TTCP). The results obtained with the Groups B and C specimens demonstrated that crystallographic transformations of HA are inevitable under certain conditions of plasma spraying. Stability of the bioceramic coating depends highly upon these minor phases, which have much higher dissolution rates compared to pure HA.[11,12,15] While appropriate manipulation of the coating parameters, such as starting powder particle composition and size, the distance of the plasma gun to the substrate, and the carrier gas, can yield high-quality coatings of nearly pure HA, the approximately 40 to 50% ACP phase is subject[7] to relatively rapid dissolution in vivo. Fundamental questions about the optimum percentage of ACP and whether the coating should remain intact in vivo or resorb are unresolved.

Conclusions

Plasma spraying of HA onto Ti-6Al-4V substrates resulted in a bioceramic coating that consisted mainly of HA, with α-TCP, ß-TCP, and TTCP as minor phases under some conditions. Approximately 40 to 50% amorphous calcium phosphate phase existed in the coatings, depending upon the deposition parameters. There were no significant differences in the crystallite sizes (ranging from about 0.02 to 0.05 µm) and the percent crystallinity values for the 3 coating groups examined. Comparison of the interplanar spacings for selected crystallographic planes with values in the ICDD standard for HA suggests that the coatings are in an uneven state of tensile strain, which is consistent with the differences in the thermal expansion coefficients of HA and Ti-6Al-4V.

Acknowledgments

The authors thank Dr William M. Johnston for assistance with the statistical analysis of the experimental data, Dr Mustafa A. Ahmetoglu for assistance with the calculations of the stresses, Ubaldo I. Soto and Professor Jerry Bigham for technical assistance and use of the x-ray diffractometer in the School of Natural Resources, and Professor Rodney J. Tettenhorst for the use of his x-ray diffractometer in the Department of Geological Sciences.

References

1. Cook SD, Kay JF, Thomas KA, Jarcho M. Interface mechanics and histology of titanium and hydroxylapatite-coated titanium for dental implant applications. Int J Oral Maxillofac Implants 1987;2:15–22.
2. De Groot K, Geesink R, Klein CPAT, Serekian P. Plasma sprayed coatings of hydroxylapatite. J Biomed Mater Res 1987;21:1375–1381.
3. Inadome T, Hayashi K, Nakashima Y, Tsumura H, Sugioka Y. Comparison of bone-implant interface shear strength of hydroxyapatite-coated and alumina-coated metal implants. J Biomed Mater Res 1995;29:19–24.

4. Lacefield WR. Hydroxylapatite coatings. In: Hench LL, Wilson J (eds). An Introduction to Bioceramics, vol 1. Singapore: World Scientific, 1993:223–238.
5. Steflik DE, Corpe RS, Lake FT, Young TR, Sisk AL, Parr GR, et al. Ultrastructural analyses of the attachment (bonding) zone between bone and implanted biomaterials. J Biomed Mater Res 1998;39:611–620.
6. Doi Y, Shibutani T, Moriwaki Y, Kajimoto T, Iwayama Y. Sintered carbonated apatites as bioresorbable bone substitutes. J Biomed Mater Res 1998;39:603–610.
7. Gross KA, Berndt CC, Herman H. Amorphous phase formation in plasma-sprayed hydroxyapatite coatings. J Biomed Mater Res 1998;39:407–414.
8. Johnson BW. HA-coated dental implants: Long-term consequences. J Calif Dent Assoc 1992;20(6):33–41.
9. Jarcho M. Calcium phosphate ceramics as hard tissue prosthetics. Clin Orthop 1981;157:259–278.
10. Klein CPAT, Patka P, van der Lubbe HBM, Wolke JGC, de Groot K. Plasma-sprayed coatings of tetracalciumphosphate, hydroxylapatite and α-TCP on titanium alloy: An interface study. J Biomed Mater Res 1991;25:53–65.
11. Klein CPAT, Wolke JGC, de Blieck-Hogervost JMA de Groot K. Calcium phosphate plasma-sprayed coatings and their stability: An *in vivo* study. J Biomed Mater Res 1994;28:909–917.
12. De Groot K, Klein CPAT, Wolke JGC, de Blieck-Hogervorst JMA. Chemistry of calcium phosphate bioceramics. In: Yamamuro T, Hench L, Wilson J (eds). Handbook of Bioactive Ceramics, vol II. Boca Raton, FL: CRC Press, 1990:3–16.
13. LeGeros RZ, LeGeros JP, Kim Y, Kijkowska R, Zheng R, Bautista C, Wong JL. Calcium phosphates in plasma-sprayed HA coatings. In: Fischman G, Clare A, Hench LL (eds). Bioceramics: Materials and Application, vol 48. Westerville, OH: American Ceramic Society, 1994: 173–189.
14. LeGeros RZ. Calcium Phosphates in Oral Biology and Medicine, monographs in Oral Science. Basel, Switzerland: Karger Press, 1991:1–3, 26–27.
15. Klein CPAT, Wolke JGC, de Blieck-Hogervorst JM, de Groot K. Features of calcium phosphate plasma-sprayed coatings: An *in vitro* study. J Biomed Mater Res 1994;28: 961–967.
16. Lacefield WR. Hydroxyapatite coatings. Ann NY Acad Sci 1988;523:72–80.
17. Kwan JY, Meffert RM. HA coatings in implant dentistry. Implant Soc 1993;3:13–16.
18. Thomas KA, Kay JF, Cook SD, Jarcho M. The effect of surface macrotexture and hydroxylapatite coating on the mechanical strengths and histological profiles of titanium implant materials. J Biomed Mater Res 1987;21: 1395–1414.
19. Cook SD, Thomas KA, Kay JF, Jarcho M. Hydroxyapatite-coated titanium for orthopedic implant applications. Clin Orthop 1988;232:225–243.
20. Søballe K, Hansen ES, Brockstedt-Rasmussen H, Pedersen CM, Bünger C. Hydroxyapatite coating enhances fixation of porous coated implants. A comparison in dogs between press fit and noninterference fit. Acta Orthop Scand 1990; 61:299–306.
21. Koch B, Wolke JGC, de Groot K. X-ray diffraction studies on plasma-sprayed calcium phosphate-coated implants. J Biomed Mater Res 1990;24:655–667.
22. Filiaggi MJ, Coombs NA, Pilliar RM. Characterization of the interface in the plasma-sprayed HA coating/Ti-6Al-4V implant system. J Biomed Mater Res 1991;25:1211–1229.
23. Ducheyne P, van Raemdonck W, Heughebaert JC, Heughebaert M. Structural analysis of hydroxyapatite coatings on titanium. Biomaterials 1986;7:97–103.
24. Ducheyne P, Radin S, Healy K, Cuckler JM. The effect of plasma spraying on the structure and properties of calcium phosphate ceramics. Trans 34th Annual ORS Meeting, 1988:50.
25. Radin SR, Ducheyne P. Plasma spraying induced changes of calcium phosphate ceramic characteristics and the effect on *in vitro* stability. J Mater Sci Mater Med 1992;3:33–42.
26. Ellies LG, Nelson DGA, Featherstone JDB. Crystallographic changes in calcium phosphates during plasma-spraying. Biomaterials 1992;13:313–316.
27. Prevey PS, Rothwell RJ. X-ray diffraction characterization of percent crystallinity and contaminants in plasma-sprayed hydroxylapatite coatings. In: Horowitz E, Parr JE (eds). Characterization and Performance of Calcium Phosphate Coatings for Implants. ASTM STP 1196. Philadelphia: American Society for Testing and Materials, 1994:63–79.
28. Ducheyne P, Healy KE. The effect of plasma-sprayed calcium phosphate ceramic coatings on the metal ion release from porous titanium and cobalt-chromium alloys. J Biomed Mater Res 1988;22:1137–1163.
29. Ducheyne P, Healy KE. Surface spectroscopy of calcium phosphate ceramic and titanium implant materials. In: Ratner BD (ed). Surface Characterization of Biomaterials. Amsterdam: Elsevier, 1988:175–192.
30. LeGeros RZ, Parsons JR, Daculsi G, Driessens F, Lee D. Materials characteristics versus in vivo behavior. In: Ducheyne P, Lemons JE (eds). Bioceramics. New York: New York Academy of Sciences, 1988:169–277.
31. Klug HP, Alexander LE. X-Ray Diffraction Procedures. Toronto: John Wiley and Sons, 1974:88–94, 635–642.
32. Foreman DW, Jakes KA. X-ray diffractometric measurement of microcrystallite size, unit cell dimensions, and crystallinity: Application to cellulosic marine textiles. Text Res J 1993;63:455–464.
33. Keller L, Rey-Fessler P. Nondestructive characterization of hydroxylapatite coated dental implants by XRD method. In: Horowitz E, Parr JE (eds). Characterization and Performance of Calcium Phosphate Coatings for Implants. ASTM STP 1196. Philadelphia: American Society for Testing and Materials, 1994:54–62.
34. Flach JS, Shimp LA, van Blitterswijk CA, de Groot K. A calibrated method for crystallinity determination of hydroxylapatite coatings. In: Horowitz E, Parr JE (eds). Characterization and Performance of Calcium Phosphate Coatings for Implants. ASTM STP 1196. Philadelphia: American Society for Testing and Materials, 1994:25–32.
35. Zaat JH. A quarter of a century of plasma spraying. Ann Rev Mater Sci 1983;13:9–42.
36. Cullity BD. Elements of X-ray Diffraction, ed 2. Reading, MA: Addison-Wesley, 1978:292–295.
37. Tufekci E. An investigation of surface and interface characteristics of plasma sprayed hydroxyapatite coated titanium dental implants [thesis]. Columbus, Ohio: The Ohio State University, 1993.
38. Brantley WA, Tufekci E, Mitchell JC, Foreman DW, McGlumphy EA. Scanning electron microscopy studies of ceramic layers and interfacial regions for calcium phosphate-coated titanium dental implants. Cells Mater 1995;5:73–82.

39. Tufekci E, Brantley WA, Mitchell JC, McGlumphy EA. Microstructures of plasma-sprayed hydroxyapatite-coated Ti-6Al-4V dental implants. Int J Oral Maxillofac Implants 1997;12:25–31.
40. Moroi HH, Okimoto K, Moroi R, Terada Y. Numeric approach to the biomechanical analysis of thermal effects in coated implants. Int J Prosthodont 1993;6:564–572.
41. Locardi B, Pazzaglia UE, Gabbi C, Profilo B. Thermal behaviour of hydroxyapatite intended for medical applications. Biomaterials 1993;14:437–441.
42. Cottrell AH. The Mechanical Properties of Matter. New York: John Wiley and Sons, 1964:134–137.
43. Grenoble DE, Katz JL, Dunn KL, Gilmore RS, Murty KL. The elastic properties of hard tissues and apatites. J Biomed Mater Res 1972;6:221–233.
44. Haase EL. The determination of lattice parameters and strains in stressed thin films using X-ray diffraction: Extensions. In: Hasek J (ed). X-ray and Neutron Structure Analysis in Materials Science. New York: Plenum Press, 1989:191–198.
45. Ljungcrantz H, Hultman L, Sundgren JE, Johansson S, Kristensen N, Schweitz JÅ, Shute CJ. Residual stresses and fracture properties of magnetron sputtered Ti films on Si microelements. J Vac Sci Technol 1993;11:543–553.
46. Kay JF. Calcium phosphate coatings for dental implants. Current status and future potential. In: Sendax VI (ed). Dent Clin North Am 1992;36:1–17.
47. Klein CPAT, Wolke JGC, de Groot K. Stability of calcium phosphate ceramics and plasma sprayed coatings. In: Hench LL, Wilson J (eds). Advanced Series in Ceramics. Vol 1: An Introduction to Bioceramics. Singapore: World Scientific, 1993:199–221.
48. Ravaglioli A, Krajewski A. Bioceramics: Materials Properties Applications. London: Chapman and Hall, 1992: 173–197.
49. Yoshimuro M, Suda H. Hydrothermal processing of hydroxyapatite: Past, present and future. In: Brown PW, Constantz B (eds). Hydroxyapatite and Related Materials. Boca Raton, FL: CRC Press, 1994:45–72.
50. Sergo V, Sbaizero O, Clarke DR. Mechanical and chemical consequences of the residual stresses in plasma sprayed hydroxyapatite coatings. Biomaterials 1997;18:477–482.
51. Callister WD Jr. Materials Science and Engineering. An Introduction. New York: John Wiley and Sons, 1994: 646–654.
52. Fairhurst CW, Hashinger DT, Twiggs SW. Glass transition temperatures of dental porcelain. J Dent Res 1981;60: 995–998.
53. Keller L. X-ray powder diffraction patterns of calcium phosphates analyzed by the Rietveld method. J Biomed Mater Res 1995;29:1403–1413.